JACS
JOURNAL OF THE AMERICAN CHEMICAL SOCIETY
pubs.acs.org/JACS
Article

Nonradiative Triplet Loss Suppressed in Organic Photovoltaic Blends with Fluoridated Nonfullerene Acceptors

Rui Wang,[#] Jianqiu Xu,[#] Lulu Fu,[#] Chunfeng Zhang,[*] Qian Li, Jia Yao, Xiaojun Li, Chenkai Sun, Zhi-Guo Zhang,[*] Xiaoyong Wang, Yongfang Li, Jing Ma,[*] and Min Xiao[*]

Cite This: J. Am. Chem. Soc. 2021, 143, 4359−4366
Read Online

ABSTRACT: In organic photovoltaic (OPV) blends, photogenerated excitons dissociate into charge-separated electrons and holes at donor/acceptor interfaces. The bimolecular recombination of spin-uncorrelated electrons and holes may cause nonradiative loss by forming the low-lying triplet excited states (T_1) via the intermediate charge-transfer triplet states. Here, we show that such a spin-related loss channel can be suppressed in the OPV blends with fluorinated nonfullerene acceptors (NFAs). By combining ultrafast optical spectroscopy and triplet sensitization measurements, the T_1 states at the acceptors have been observed to generate from the charge-separated electrons and holes in the OPV blends with a same polymer donor and two sets of NFAs with and without fluorination. The triplet formation is largely suppressed and the lifetime of charge carrier is markedly prolonged in the blends with fluorinated NFAs. The fluorination effect on the charge dynamics can be ascribed to the modified energy alignment between the triplet excited states of charge-transfer and locally excited characters as supported by quantum chemical computation. Our findings explain the mechanism responsible for the improved photocurrent generation in the OPV blends with fluorinated NFAs, suggesting that manipulating the energy landscape of triplet excited states is a promising strategy for further optimizing OPV devices.

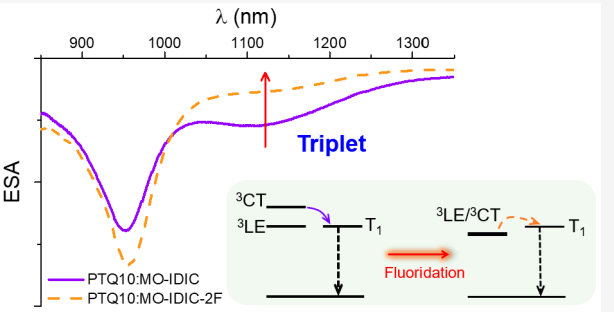

INTRODUCTION

Organic solar cells (OSCs) convert light into electricity using the donor:acceptor (D:A) bulk heterojunction structure.[1−7] In comparison to inorganic devices, the overall power conversion efficiency (PCE) of OSCs is limited by additional nonradiative recombination loss.[4,7−13] During photocharge generation, the interfacial energy offset required for dissociation of photoexcited excitons is generally much higher for OSCs due to the strong binding energy in organic molecules.[2] Post charge generation, the relatively large energetic disorder and the nonradiative recombination cause additional energy losses through phonon-mediated or spin-mediated pathways.[9,12,14−21] Interestingly, these loss channels can be partially relieved in the state-of-the-art OSCs with nonfullerene acceptors (NFAs).[22−26] Owing to the intramolecular electron push−pull effect, the spectral coverage of NFAs is generally much broader.[4] In most high-performance polymer/NFA blends, efficient charge separation has been enabled with remarkably low energy offset at the D/A interface,[8,27−34] which largely reduces the interfacial energy loss during charge separation. By using small-molecule NFAs with torsion-free molecular conformation, the energy loss related to energetic disorder can be mitigated.[20,22] These technical advances result in remarkable improvements for device performance with certified PCE above 17%.[35] To further optimize the OPV devices, it is necessary to better understand and suppress the nonradiative recombination losses.

Fluorination has been established as a facile but highly efficient way to improve the device performance of OSCs with NFAs.[5,36,37] So far, most highly efficient OPV blends (PCEs > 15%) usually contain the photovoltaic material with fluorine substituents.[27,28,38−41] Introducing fluorine atoms to the side chain of NFAs has added a 1−2% increase of PCEs in multiple material systems. These improvements have been generally ascribed to the effects of the energy level alignment optimized for interfacial charge separation and charge carrier transport promoted by the morphology modulation.[19,37,42] Nevertheless, it remains elusive whether and how the fluorination affects the dynamics of nonradiative recombination loss. In this work, we show that the fluorination of NFAs can suppress the spin-related pathway of nonradiative loss in OPV devices with NFAs. As shown in Figure 1a, free charge pairs resulting from charge separation at the D/A interface may undergo

Received: December 27, 2020
Published: March 15, 2021

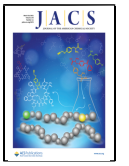

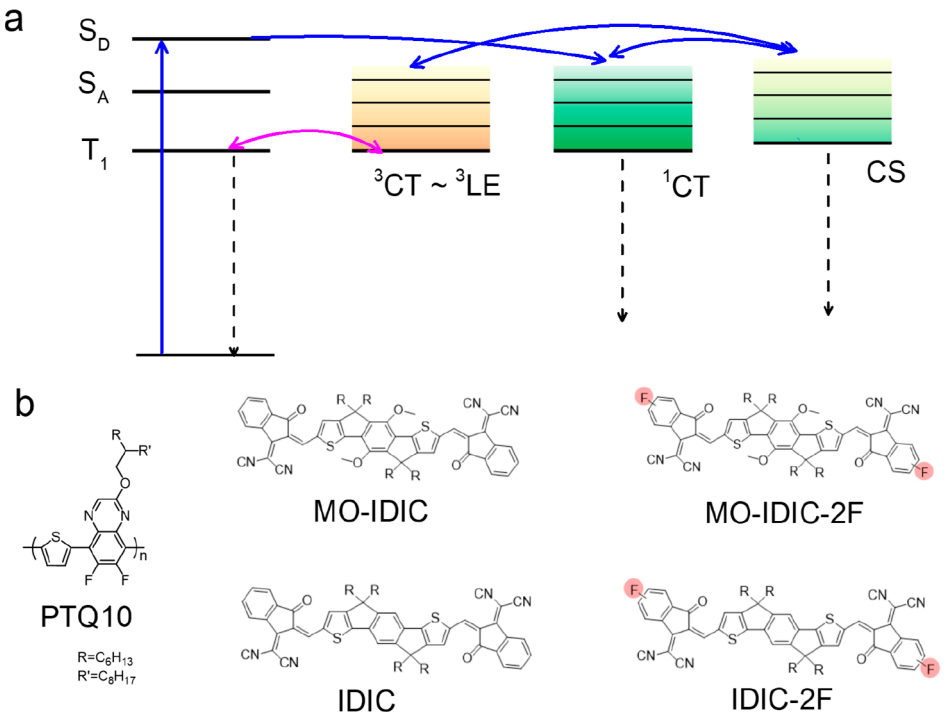

Figure 1. Charge generation and recombination routes in an OPV blend and molecular structures. (a) Schematic diagram of the dynamics of triplet excited states in bulk-heterojunctions. (b) Molecular structures of polymer donor (PTQ 10) and two sets of small molecule acceptors without (MO-IDIC, IDIC) and with (MO-IDIC-2F, IDIC-2F) fluorination treatment used in this study.

bimolecular recombination to charge-transfer (CT) states with either spin singlet or triplet characters; interfacial triplet charge-transfer (^{3}CT) states then convert into the lowest-lying locally excited triplet (T_1) states in the acceptors, which may be annihilated by the charges in the blend.[14,16,20]

To investigate the effect of fluorination of the NFAs and the spin-related nonradiative loss in the OSCs, we study the charge dynamics in the OSCs based on two sets of indacenodithiophen (IDT)-based NFAs without (MO-IDIC, IDIC) and with (MO-IDIC-2F, IDIC-2F) fluorine substituents[43] blended with a same polymer donor (PTQ10)[44] by combining broadband transient absorption (TA) spectroscopic and quantum chemical computation methods. While charge generation dynamics are similar in the blend films with NFAs without and with fluorination, the recombination dynamics show markedly differences with triplet formation strongly suppressed in the blends with fluorinated NFAs. The fluorination effect on the triplet generation dynamics can be ascribed to the modified energy alignment between the triplet excited states. The triplet loss channel is largely suppressed in the blends with fluoridated NFAs, which is responsible for the improved photocurrent generation and output PCEs. The finding in this work suggests that manipulating the energy landscape of triplet excited states by molecular design is a viable route to promote the performance of OSCs.

MATERIALS AND METHODS

Sample Preparation. Acceptors IDIC and IDIC-2F were purchased from Solarmer Materials Inc. and Hyper Inc. respectively. The donor PTQ10 and acceptors MO-IDIC and MO-IDIC-2F were synthesized according to the procedures reported previously.[43]

Film samples for TA measurement were fabricated by spin coating on quartz substrates. For blend samples, the donor:acceptor ratio was 1:1 (w/w). After spin coating, blended film samples were annealed in argon atmosphere at 140, 120, or 110 °C for 5 min for different acceptors according to the optimized conditions of device fabrication. For triplet sensitization measurements, the solution samples with a 1:4 weight ratio of the sensitizer PtOEP and acceptors were coated onto the substrates. Samples were kept in nitrogen atmosphere for optical characterizations.

Optical Characterization. TA spectroscopy was conducted by employing a Ti:sapphire regenerative amplifier (Libra, Coherent Inc.) at 800 nm having a repetition rate of 1 kHz and pulse duration of 90 fs. An optical parametric amplifier (OperA Solo, Coherent Inc.) pumped by the regenerative amplifier was used to generate the pump beams with tunable wavelengths. The probe beams of supercontinuum in the visible and infrared wavelength ranges were generated by focusing a small portion of the femtosecond laser beam onto a 3 mm thick sapphire plate or a 5 mm thick yttrium aluminum garnet (YAG) plate, respectively. The spectra were acquired using a silicon CCD (S7030-1006, Hamamatsu Ltd.) for the visible range and an InGaAs CCD (G11608, Hamamatsu) for the infrared range with a monochromator (Acton 2358, Princeton Instrument). The signal of differential transmission ($\Delta T/T$) was acquired pulse to pulse at 1 kHz enabled by a custom-built control board from Entwicklungsbuero Stresing. The signal-to-noise ratio reaches 5×10^{-5} after averaging 1000 couples of pump-on and pump-off spectra. For time delays longer than 4 ns, the pump laser was replaced by a pulsed laser diode emitted at 670 nm (LDH-P-C-670M, Picoquant). The time delay between the two lasers was synchronized and enabled by a digital delay generator (DG645, Stanford Research System).

Photoinduced absorption (PIA) spectra were measured under a cw-pump pulse-probe configuration. A He−Ne laser (HNL 050L, Thorlabs) at 632.8 nm was used to pump the samples, and the probe beam was the supercontinuum used in visible and infrared TA. The pump beam was modulated by an optical chopper at 500 Hz. For organic solar cells, the characteristic carrier lifetime is less than 1 ms and charge transfer process finishes in less than 1 ns, differential transmission was detected as the signal of free carriers. Excitation fluence was 60 mW/cm^2 to keep the same excitation density as AM1.5 in visible range.

Quantum Chemical Computation. Density function theory (DFT) and time dependent DFT were employed to simulate the

https://dx.doi.org/10.1021/jacs.0c13352
J. Am. Chem. Soc. 2021, 143, 4359−4366

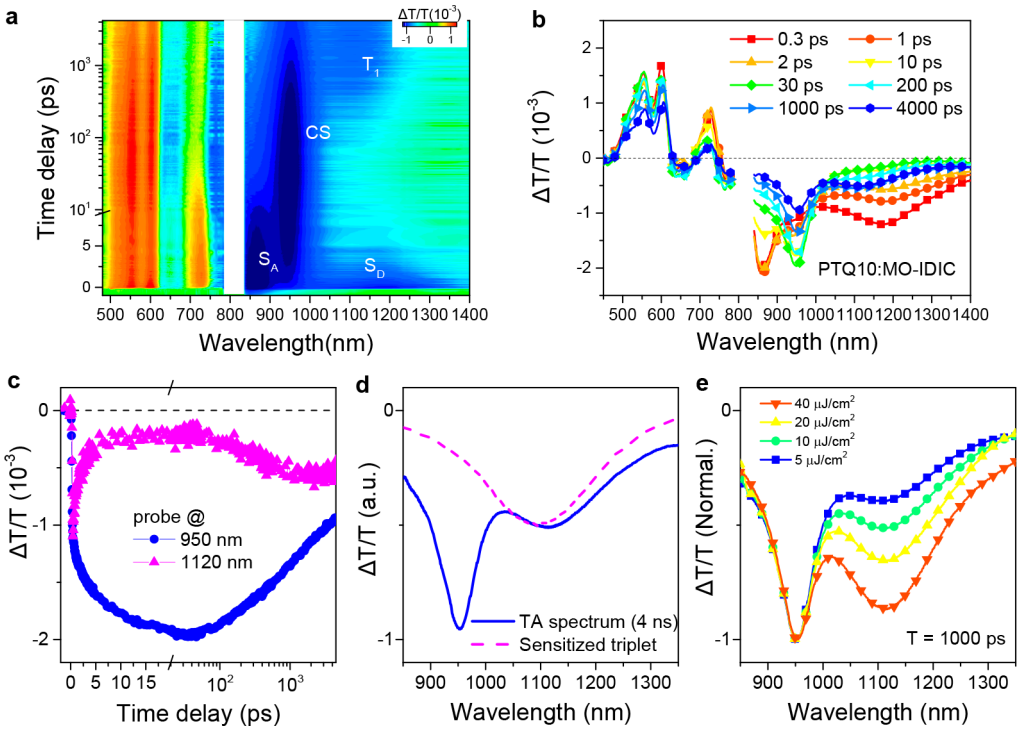

Figure 2. Triplet generation dynamics in a blend film of PTQ10:MO-IDIC. (a) Contour plot of TA data recorded from the blend film at different time delays and different probe wavelengths. The data are acquired with pump at 500 nm of 5 μJ/cm^2. (b) TA spectra recorded from the blend film at different time delays. (c) Kinetic curves of ESA signals at 950 and 1120 nm, respectively. (d) TA spectrum of the PTQ10:MO-IDIC blend recorded at the delay of 4 ns is compared with the absorption spectrum of the triplet state of MO-IDIC characterized by triplet sensitization (Figure S6). (e) Normalized TA spectra measured at different pump fluences.

geometric structures and energy levels of singlet ground state and triplet excited state, respectively, using GAUSSIAN 16 program. The optimized structures of the triplet excited states were illustrated by using Multiwfn 3.3.9. More details are available in the Supporting Information (SI).

RESULTS AND DISCUSSION

Charge Generation Dynamics. The chemical structures of materials used in this study are illustrated in Figure 1b. The polymer donor PTQ10 is selected in this study with a relatively simple molecular structure.[44] The PCEs of the optimized devices with the blend films using the NFAs of MO-IDIC and IDIC increase from 11.0% and 11.6% to 13.3% and 12.1%, respectively, when the NFAs are fluorinated to be MO-IDIC-2F and IDIC-2F.[43] As summarized in the Supporting Information (Table S1), the increased PCEs can be attributed to the suppressed loss of free charges. We conduct TA measurements to uncover the carrier dynamics underlying the fluorination effect of device performance. The pump wavelength is 500 nm which can excite both the donor PTQ10 and nonfullerene acceptors (Figures S1 and S2), and the excitation fluence is 5 μJ/cm^2 to avoid exciton annihilation at the early stage (Figure S3).

The charge generation processes are similar in the blend systems. Figure 2a presents the fs-resolved TA spectra of a blend film of PTQ10:MO-IDIC probed in the wavelength range from 450 to 1400 nm. Simultaneously upon photon excitation, two excited-state absorption (ESA) bands at 860 and 1180 nm emerge (Figure 2b). The two ESA bands can be assigned to the primarily excited singlet states of MO-IDIC and PTQ10, respectively, which are also present in the TA spectra recorded from the neat films of acceptor MO-IDIC and donor PTQ-10 (Figure S2). The hole transfer and electron transfer processes are observed with the faster decay of the ESA features at 860 and 1180 nm, together with the correlated buildup of the ESA feature at 950 nm within 30 ps (Figures 2b and S2). The generated ESA feature at 950 nm is absent in the neat films of either acceptor or donor, which persists together with the ground state bleaching (GSB) features of the donor and acceptor, so that it can be naturally assigned to the interfacial CT states. Following the interfacial charge transfer, we observe a slight red-shift in the ESA signal around 950 nm in the time scale from 30 to 200 ps (Figure S4), which is a signature of further charge separation of the interfacial CT states. The formation of free charges induces a change of the local Stark effect, resulting in the spectral shift of the ESA feature.[45] To confirm the assignment, we characterize the absorption spectral feature of free charges using the PIA measurement (Figure S5) upon continuous wave excitation. The long-lived PIA feature of free charges is comparable to the observed features in TA spectra, confirming the assignment of charge separated states.[46−48]

Triplet Formation. In OPV devices, the separated free charges are collected by the electrodes with the aid of electron and hole transport layers to generate the photocurrent.[49] Nevertheless, the process of photocurrent generation competes against loss channels of charge recombination.[13,46,50] At a long time scale (200 ps −4 ns), the ESA at 950 nm starts to decay and a new ESA feature at 1120 nm builds up gradually (Figure 2a,c), suggesting the formation of a new excited-state species during the recombination of free charges. As shown in Figure 1a, the reversal process of charge separation may result in the formation of both ^{1}CT and ^{3}CT states at the D/A interface through the bimolecular recombination process of free charges.

https://dx.doi.org/10.1021/jacs.0c13352
J. Am. Chem. Soc. 2021, 143, 4359−4366

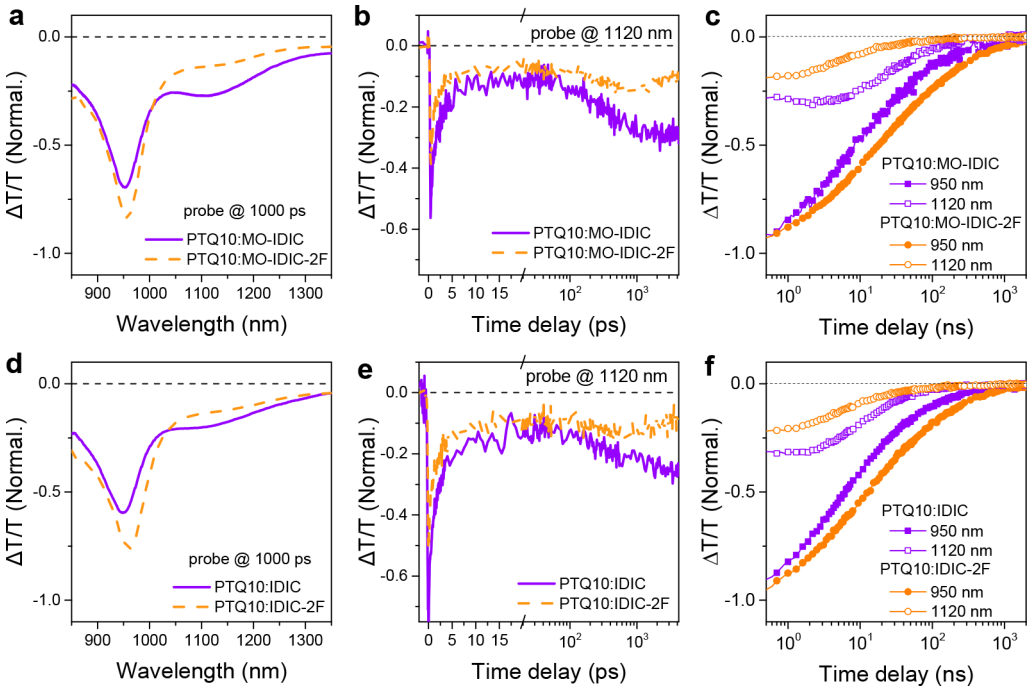

Figure 3. Fluorination effect on triplet generation dynamics. (a) TA spectra at the delay of 1 ns, (b) fs-resolved kinetic curves probed at 1120 nm, and (c) ns-resolved kinetic curves probed at 950 and 1120 nm recorded from the blend samples with the acceptors of MO-IDIC and MO-IDIC-2F, respectively. Panels (d)−(f) are the same as (a)−(c) but for the acceptors IDIC and IDIC-2F, respectively. The fs-resolved TA data are acquired with pump at 500 nm of 5 μJ/cm^2, while the ns-resolved TA data are acquired with pump at 670 nm of 2 μJ/cm^2. The signals are normalized at the maximal amplitude of the ESA signal at 950 nm.

The ^{3}CT states may convert to the low-lying triplet T_1 state which is the triplet state of NFA of MO-IDIC in the blend film of PTQ10:MO-IDIC. The spectral feature of triplet state of MO-IDIC characterized by triplet sensitization measurements agrees well with the newly generated ESA feature centered at 1120 nm (Figure 2d), suggesting the formation of T_1 state at the NFA during the bimolecular recombination of free charges. The assignment is further supported by the pump-fluence dependences of carrier dynamics. With increasing pump fluence, the decay rate of the signal probed at 950 nm and the growth rate of the signal probed at 1120 nm increase correlatedly (Figure S7). Moreover, the spectral feature of the T_1 state becomes more pronounced at higher pump fluences (Figure 2e), indicating that the bimolecular recombination of free charges dominates the triplet formation in the PTQ10:MO-IDIC blend. The localized triplet undergoes the triplet-charge annihilation process, resulting in additional nonradiative loss.[14] The triplet generation is also observed when the acceptor is selectively excited at 700 nm, suggesting that it is a common channel in the photocharge generation process (Figure S8). The lifetime parameters of the different processes can be evaluated by the global fitting analysis (Figure S9).

Effect of Fluorination on Triplet Dynamics. In all four blend samples, the triplet generation has been observed, implying that the nonradiative triplet loss channel is common in OPV systems with NFAs. Nevertheless, the triplet generation dynamics show marked differences in the blends with and without fluorinated acceptors as compared in Figure 3. In comparison with the blend PTQ10:MO-IDIC, the charge generation dynamics are similar in the blend PTQ10:MO-IDIC-2F (Figure S10). Notably, the ESA feature of triplet at 1120 nm is markedly reduced in the TA spectrum of the blend PTQ10:MO-IDIC-2F on a longer time scale (Figure 3a). The delayed-rise component in the kinetics probed at 1120 nm is also markedly reduced (Figure 3b), while the signal of free charges probed at 950 nm persists to a much longer time scale. Similar fluorinated effect is also observed in the blend films with NFAs of IDIC and IDIC-2F (Figures 3d,e and S11). These results indicate that the triplet formation is significantly reduced when the NFA is fluoridated.

The fluorination effect is also manifested of the free charge dynamics in the nanosecond time scale. Figure 3c compares the ns-resolved TA results recorded from the blend films of PTQ10:MO-IDIC and PTQ10:MO-IDIC-2F. In the blend with fluorinated acceptor, the signals of free charges probed at 950 nm persist for a much longer time, suggesting that the reduced triplet formation is essential for lifetime extension of free charges in the blends, which is beneficial for charge collection. Similar fluorination effects are observed in the blend systems with NFAs of IDIC and IDIC-2F (Figure 3f). These corroborated results suggest that fluorinating NFAs can efficiently suppress the triplet formation, extend the lifetime of free charges, and consequently improve quantum efficiency of photocurrent generation.

Triplet Level Alignment. Next, we discuss the possible mechanisms underlying the fluorination effect on the triplet channel in these OPV blend films. The probability of triplet formation is susceptible to the bimolecular recombination of free charges. In principle, bimolecular recombination is more efficient in the system with higher mobility which has a higher chance for the encounter of positive and negative polarons.[14] Nevertheless, the transport measurements suggest that the charge mobilities are higher in the blends with fluorinated NFAs,[43] which cannot explain the suppressed triplet formation in these blends.

https://dx.doi.org/10.1021/jacs.0c13352
J. Am. Chem. Soc. 2021, 143, 4359−4366

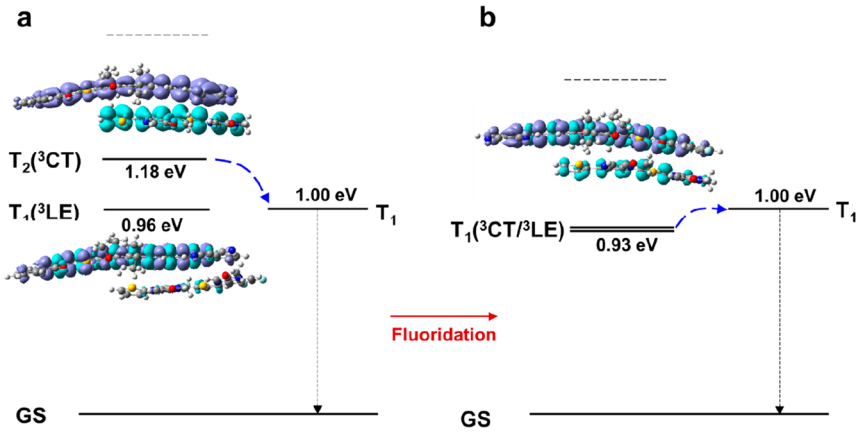

Figure 4. Schematic diagram of fluorination effect on the energy alignment of triplet excited states. Calculated electron (purple) and hole (blue) distribution of the T_1 and T_2 in the D:A dimers with (a) MO-IDIC and (b) MO-IDIC-2F. In the blends with fluorinated NFAs, the lowest triplet state at the D/A interface is more like a ^{3}CT state which is energetically unfavorable for T_1 formation. (LE, local excited state; GS, ground state; CT, charge-transfer excited state; T_1, lowest triplet state in the acceptors.)

It has been well established that fluorine substitution slightly modifies the oxidation and reduction potential of conjugated molecules, which may change the energy alignment between the locally excited (LE) and interfacial CT states.[51,52] To gain more insight, we survey the electronic structures of the triplet excited states in these systems by quantum chemical computations. We model the systems with dimer structures consisting of these NFAs and two repetition units of PTQ10 (Figures S12−S19). The lowest-lying triplet levels of acceptors are considered as the T_1 states. The geometric structures of the triplet excited states of the energetic lowest-lying states are optimized by time-dependent density functional theory (Table S2). As a result of the interfacial D:A coupling, the calculated adiabatic triplet states are hybridized by the ^{3}CT state and locally excited triplet (^{3}LE) state at the acceptor site in the D:A dimer. For the neat NFAs, the effect of fluorination on the triplet energy level is insignificant (Table S3). In the D:A dimers, fluorination of NFAs markedly affects the energy landscapes and the orbital features of the low-lying triplet states (Figures 4 and S16; Table S3).[53] Our computational results of the model system of PTQ10:MO-IDIC (Figure 4a) indicate that the lowest-lying two triplet levels are dominated by the ^{3}LE and ^{3}CT characters, respectively. The ^{3}CT state is higher than the T_1 state, which is favorable for the formation of T_1 state. In contrast, for the model of PTQ10:MO-IDIC-2F (Figure 4b), the lowest-lying triplet levels are heavily mixed with the ^{3}LE and ^{3}CT characters, being more stabilized with lower transition energies in comparison with the blend prior to fluorination. Similar results of fluorination effect are also obtained for the blends of PTQ10: IDIC and PTQ10:IDIC-2F (Table S3). While the exact energies of the triplet states in the blend films may vary from the computational values due to the complicated molecular packing structures (Figures S18 and S19), the trend predicted by the quantum chemical calculation is instructive for understanding the fluorination effect. The relatively large electronegativity of fluorine may modify the packing structure at the D/A interface and lower the energy of triplet states by mixing ^{3}LE and ^{3}CT characters (Figure 1a). The energy alignment of triplet excited states is less energetically favorable for triplet formation in the blends with the fluorinated acceptor, which is responsible for the observed fluorination effect on the dynamics of triplet generation and charge recombination.[52] In principle, both forward and backward transfer processes are possible to establish the dynamic equilibrium between the populations at the ^{3}CT to ^{3}LE states if their energy gap is comparable to the thermal activation energy. The equilibrium, controllable by the energy alignment, may shift to the state with faster deexcitation, which can be potentially manipulated to optimize an OPV device.

In short, fluorination of NFAs may change multiple factors including the morphology, the dielectric constant, and the energy level alignment. The fluorination of NFA may modify the molecular packing and alignment inside the acceptor domains and at the donor/acceptor interfaces. The morphology changes caused by fluorination in the acceptor domains may enhance the charge carrier mobility. In principle, the improved charge transport increases the bimolecular recombination, resulting in enhanced triplet generation in the blends with fluorinated NFAs, which, however, is contrary to the experimental results.[43] On the other hand, the molecular stacking at the donor−acceptor interfaces modified by the fluorination of the acceptor may affect the intermolecular interaction, resulting in the change of energy level alignment, which can explain the observed fluorination effect on the triplet formation (e.g., Figure 4). Moreover, the dielectric constant is possibly modified by the fluorination of NFAs, which, is unlikely to be a key effect for the enhanced triplet formation as the energies of the triplet levels are insensitive to the dielectric constant (Table S2).

Device Implication. In general, bimolecular recombination of free charges is susceptible to the charge density.[14] It is under debate whether the loss channel observed under ultrashort pulse excitation is truly functional in OPV devices under solar illumination. For AM1.5 illumination, the charge density in a working device is on the order of $\sim 10^{16}$ cm^{-3}, which is usually one order lower than the excitation condition of the TA experiment ($\sim 10^{17}$ cm^{-3}).[16,54] To approach the free charge dynamics and the triplet loss channel at solar illumination conditions, we perform the ns-resolved TA spectroscopic measurements with improved sensitivity by varying the excitation density from 3×10^{17} to 3×10^{16} cm^{-3} (the pump fluence from 2 to 0.2 μJ/cm^2 at 670 nm). As shown in Figure S20, the lifetime of free charges probed at 950 nm is extended at lower pump fluences with reduced bimolecular recombination. With an excitation density of $3 \times$

https://dx.doi.org/10.1021/jacs.0c13352
J. Am. Chem. Soc. 2021, 143, 4359−4366

10^{16} cm^{-3}, triplet signals probed at 1120 nm are recognizable in these blends. In the blends, the lifetimes of the T_1 signals at 1120 nm are significantly shortened with increasing pump fluence, which is a signature of the loss caused by the triplet-charge interaction. Moreover, the lifetime of free charge in the blend with fluorinated acceptor is always much longer than that in the blend without fluorinated acceptor under the same excitation density. These results confirm that fluorination of the acceptor can suppress the triplet loss channel and extend the lifetime of free charge, which is also critical for the device performance under working condition.[54]

In working devices, fluorination of NFAs can efficiently suppress the triplet formation, which is manifested with marked improvement of the short-circuit current. In the devices with fluorinated NFAs, the short-circuit currents increase more than 2 mA/cm^2 which is a remarkable improvement since the absorption spectral coverages of OPV blends remain nearly unchanged (Table S1). In principle, suppressing the nonradiative loss channel should increase the open-circuit voltage of OPV devices if other factors are the same. However, in the devices with fluorinated NFAs, the values of open-circuit voltages slightly drop, which is probably caused by the modified energy of CT states due to the down-shifted LUMO of the fluorinated NFAs.[37] The improvement of PCEs in the devices with the fluorinated NFAs is attributed to the significantly improved short-circuit current. Toward an ideal device, a new strategy is expected to optimize the energy alignment of triplet energy levels without sacrificing the voltage.

CONCLUSION

In summary, we have demonstrated that, in the OPV blends with NFAs, the triplet loss channel of free charges can be efficiently suppressed by introducing fluorine substituents to the terminal acceptor unit of NFAs. The down-shifting of interfacial triplet excited states by fluorination plays a pivotal role in suppressing triplet exciton formation. These results inspire us to take the energy level arrangement of triplet excited states into consideration when designing the active layer materials. In addition, to balance the trade-off between V_{OC} and the triplet loss, structural optimization of the NFAs to reduce the exchange energy can make the energy alignment of triplet excitons suitable to alleviate the triplet loss in high performance organic solar cells.

ASSOCIATED CONTENT

Supporting Information

The Supporting Information is available free of charge at https://pubs.acs.org/doi/10.1021/jacs.0c13352.

Absorption spectra of the donor (PTQ10) and NFA (MO-IDIC, MO-IDIC-2F, IDIC, IDIC-2F) films; TA data of PTQ10 and MO-IDIC neat films; Excitation fluence-dependent TA measurements; PIA spectrum of PTQ10:MO-IDIC; Triplet sensitization experiments; Power dependent triplet generation dynamics; TA data of PTQ10:MO-ITIC upon optical excitation at 700 nm; Global analysis of the excited state dynamics; TA data of PTQ10:MO-IDIC-2F, PTQ10:IDIC and PTQ10: IDIC-2F blends; Ns-resolved power dependence dynamics of free charges; calculation details and results (PDF)

AUTHOR INFORMATION

Corresponding Authors

Chunfeng Zhang − *National Laboratory of Solid State Microstructures, School of Physics, and Collaborative Innovation Center for Advanced Microstructures, Nanjing University, Nanjing 210093, China;* orcid.org/0000-0001-9030-5606; Email: cfzhang@nju.edu.cn

Zhi-Guo Zhang − *Beijing National Laboratory for Molecular Sciences, CAS Key Laboratory of Organic Solids, Institute of Chemistry, Chinese Academy of Sciences, Beijing 100190, China; State key Laboratory of Chemical Resource Engineering, College of Materials Science and Engineering, Beijing University of Chemical Technology, Beijing 100029, China;* orcid.org/0000-0003-4341-7773; Email: zgzhangwhu@iccas.ac.cn

Jing Ma − *Institute of Theoretical and Computational Chemistry, Key Laboratory of Mesoscopic Chemistry of MOE, School of Chemistry and Chemical Engineering, Nanjing University, Nanjing 210093, China;* orcid.org/0000-0001-5848-9775; Email: majing@nju.edu.cn

Min Xiao − *National Laboratory of Solid State Microstructures, School of Physics, and Collaborative Innovation Center for Advanced Microstructures, Nanjing University, Nanjing 210093, China; Department of Physics, University of Arkansas, Fayetteville, Arkansas 72701, United States*; Email: mxiao@uark.edu

Authors

Rui Wang − *National Laboratory of Solid State Microstructures, School of Physics, and Collaborative Innovation Center for Advanced Microstructures, Nanjing University, Nanjing 210093, China*

Jianqiu Xu − *National Laboratory of Solid State Microstructures, School of Physics, and Collaborative Innovation Center for Advanced Microstructures, Nanjing University, Nanjing 210093, China*

Lulu Fu − *Institute of Theoretical and Computational Chemistry, Key Laboratory of Mesoscopic Chemistry of MOE, School of Chemistry and Chemical Engineering, Nanjing University, Nanjing 210093, China*

Qian Li − *National Laboratory of Solid State Microstructures, School of Physics, and Collaborative Innovation Center for Advanced Microstructures, Nanjing University, Nanjing 210093, China*

Jia Yao − *Beijing National Laboratory for Molecular Sciences, CAS Key Laboratory of Organic Solids, Institute of Chemistry, Chinese Academy of Sciences, Beijing 100190, China; State key Laboratory of Chemical Resource Engineering, College of Materials Science and Engineering, Beijing University of Chemical Technology, Beijing 100029, China*

Xiaojun Li − *Beijing National Laboratory for Molecular Sciences, CAS Key Laboratory of Organic Solids, Institute of Chemistry, Chinese Academy of Sciences, Beijing 100190, China*

Chenkai Sun − *Beijing National Laboratory for Molecular Sciences, CAS Key Laboratory of Organic Solids, Institute of Chemistry, Chinese Academy of Sciences, Beijing 100190, China*

Xiaoyong Wang − *National Laboratory of Solid State Microstructures, School of Physics, and Collaborative Innovation Center for Advanced Microstructures, Nanjing*

https://dx.doi.org/10.1021/jacs.0c13352
J. Am. Chem. Soc. 2021, 143, 4359−4366

University, Nanjing 210093, China; orcid.org/0000-0003-1147-0051

Yongfang Li − *Beijing National Laboratory for Molecular Sciences, CAS Key Laboratory of Organic Solids, Institute of Chemistry, Chinese Academy of Sciences, Beijing 100190, China;* orcid.org/0000-0002-2565-2748

Complete contact information is available at: https://pubs.acs.org/10.1021/jacs.0c13352

Author Contributions

[#]R.W., J.X., and L.F. contributed equally to this work.

Notes

The authors declare no competing financial interest.

■ ACKNOWLEDGMENTS

This work is supported by the National Key R&D Program of China (Grant Nos. 2017YFA0303700 and 2018YFA0209101), the National Science Foundation of China (Grant NOs. 21922302, 21873047, 11904168, 91833305, 91850105, and 22033004), Science and Technology Project of Jiangsu Province of China (BK20190290), the Priority Academic Program Development of Jiangsu Higher Education Institutions (PAPD), and the Fundamental Research Funds for the Central University. The authors acknowledge Dr. Xuewei Wu for providing technical assistance.

■ REFERENCES

(1) Yu, G.; Gao, J.; Hummelen, J. C.; Wudl, F.; Heeger, A. J. Polymer Photovoltaic Cells-Enhanced Efficiencies Via a Network of Internal Donor-Acceptor Heterojunctions. *Science* **1995**, *270*, 1789.

(2) Clarke, T. M.; Durrant, J. R. Charge Photogeneration in Organic Solar Cells. *Chem. Rev.* **2010**, *110*, 6736.

(3) Cheng, P.; Li, G.; Zhan, X.; Yang, Y. Next-Generation Organic Photovoltaics Based on Non-Fullerene Acceptors. *Nat. Photonics* **2018**, *12*, 131.

(4) Hou, J.; Inganas, O.; Friend, R. H.; Gao, F. Organic Solar Cells Based on Non-Fullerene Acceptors. *Nat. Mater.* **2018**, *17*, 119.

(5) Yan, C.; Barlow, S.; Wang, Z.; Yan, H.; Jen, A. K. Y.; Marder, S. R.; Zhan, X. Non-Fullerene Acceptors for Organic Solar Cells. *Nat. Rev. Mater.* **2018**, *3*, 18003.

(6) Lu, L.; Zheng, T.; Wu, Q.; Schneider, A. M.; Zhao, D.; Yu, L. Recent Advances in Bulk Heterojunction Polymer Solar Cells. *Chem. Rev.* **2015**, *115*, 12666.

(7) Qian, D.; Zheng, Z.; Yao, H.; Tress, W.; Hopper, T. R.; Chen, S.; Li, S.; Liu, J.; Chen, S.; Zhang, J.; Liu, X.-K.; Gao, B.; Ouyang, L.; Jin, Y.; Pozina, G.; Buyanova, I. A.; Chen, W. M.; Inganas, O.; Coropceanu, V.; Bredas, J.-L.; Yan, H.; Hou, J.; Zhang, F.; Bakulin, A. A.; Gao, F. Design Rules for Minimizing Voltage Losses in High-Efficiency Organic Solar Cells. *Nat. Mater.* **2018**, *17*, 703.

(8) Sun, C.; Pan, F.; Chen, S.; Wang, R.; Sun, R.; Shang, Z.; Qiu, B.; Min, J.; Lv, M.; Meng, L.; Zhang, C.; Xiao, M.; Yang, C.; Li, Y. Achieving Fast Charge Separation and Low Nonradiative Recombination Loss by Rational Fluorination for High-Efficiency Polymer Solar Cells. *Adv. Mater.* **2019**, *31*, 1905480.

(9) Chow, P. C.; Gelinas, S.; Rao, A.; Friend, R. H. Quantitative Bimolecular Recombination in Organic Photovoltaics through Triplet Exciton Formation. *J. Am. Chem. Soc.* **2014**, *136*, 3424.

(10) Ferguson, A. J.; Kopidakis, N.; Shaheen, S. E.; Rumbles, G. Dark Carriers, Trapping, and Activation Control of Carrier Recombination in Neat P3ht and P3ht:Pcbm Blends. *J. Phys. Chem. C* **2011**, *115*, 23134.

(11) Hilczer, M.; Tachiya, M. Unified Theory of Geminate and Bulk Electron−Hole Recombination in Organic Solar Cells. *J. Phys. Chem. C* **2010**, *114*, 6808.

(12) Schwarz, K. N.; Geraghty, P. B.; Jones, D. J.; Smith, T. A.; Ghiggino, K. P. Suppressing Subnanosecond Bimolecular Charge Recombination in a High-Performance Organic Photovoltaic Material. *J. Phys. Chem. C* **2016**, *120*, 24002.

(13) Etzold, F.; Howard, I. A.; Mauer, R.; Meister, M.; Kim, T.-D.; Lee, K.-S.; Baek, N. S.; Laquai, F. Ultrafast Exciton Dissociation Followed by Nongeminate Charge Recombination in Pcdtbt:Pcbm Photovoltaic Blends. *J. Am. Chem. Soc.* **2011**, *133*, 9469.

(14) Lakhwani, G.; Rao, A.; Friend, R. H. Bimolecular Recombination in Organic Photovoltaics. *Annu. Rev. Phys. Chem.* **2014**, *65*, 557.

(15) Chang, W.; Congreve, D. N.; Hontz, E.; Bahlke, M. E.; McMahon, D. P.; Reineke, S.; Wu, T. C.; Bulovic, V.; Van Voorhis, T.; Baldo, M. A. Spin-Dependent Charge Transfer State Design Rules in Organic Photovoltaics. *Nat. Commun.* **2015**, *6*, 6415.

(16) Rao, A.; Chow, P. C.; Gelinas, S.; Schlenker, C. W.; Li, C. Z.; Yip, H. L.; Jen, A. K.; Ginger, D. S.; Friend, R. H. The Role of Spin in the Kinetic Control of Recombination in Organic Photovoltaics. *Nature* **2013**, *500*, 435.

(17) Di Nuzzo, D.; Aguirre, A.; Shahid, M.; Gevaerts, V. S.; Meskers, S. C. J.; Janssen, R. A. J. Improved Film Morphology Reduces Charge Carrier Recombination into the Triplet Excited State in a Small Bandgap Polymer-Fullerene Photovoltaic Cell. *Adv. Mater.* **2010**, *22*, 4321.

(18) Etzold, F.; Howard, I. A.; Forler, N.; Melnyk, A.; Andrienko, D.; Hansen, M. R. Laquai‡, F., Sub-Ns Triplet State Formation by Non-Geminate Recombination in Psbtbt:Pc70bm and Pcpdtbt:Pc60bm Organic Solar Cells. *Energy Environ. Sci.* **2015**, *8*, 1511.

(19) Stuart, A. C.; Tumbleston, J. R.; Zhou, H.; Li, W.; Liu, S.; Ade, H.; You, W. Fluorine Substituents Reduce Charge Recombination and Drive Structure and Morphology Development in Polymer Solar Cells. *J. Am. Chem. Soc.* **2013**, *135*, 1806.

(20) Menke, S. M.; Cheminal, A.; Conaghan, P.; Ran, N. A.; Greehnam, N. C.; Bazan, G. C.; Nguyen, T. Q.; Rao, A.; Friend, R. H. Order Enables Efficient Electron-Hole Separation at an Organic Heterojunction with a Small Energy Loss. *Nat. Commun.* **2018**, *9*, 277.

(21) Dimitrov, S. D.; Wheeler, S.; Niedzialek, D.; Schroeder, B. C.; Utzat, H.; Frost, J. M.; Yao, J.; Gillett, A.; Tuladhar, P. S.; McCulloch, I.; Nelson, J.; Durrant, J. R. Polaron Pair Mediated Triplet Generation in Polymer/Fullerene Blends. *Nat. Commun.* **2015**, *6*, 6501.

(22) Liu, S.; Yuan, J.; Deng, W.; Luo, M.; Xie, Y.; Liang, Q.; Zou, Y.; He, Z.; Wu, H.; Cao, Y. High-Efficiency Organic Solar Cells with Low Non-Radiative Recombination Loss and Low Energetic Disorder. *Nat. Photonics* **2020**, *14*, 300.

(23) Lin, Y.; Wang, J.; Zhang, Z.-G.; Bai, H.; Li, Y.; Zhu, D.; Zhan, X. An Electron Acceptor Challenging Fullerenes for Efficient Polymer Solar Cells. *Adv. Mater.* **2015**, *27*, 1170.

(24) Wang, R.; Yao, Y.; Zhang, C.; Zhang, Y.; Bin, H.; Xue, L.; Zhang, Z. G.; Xie, X.; Ma, H.; Wang, X.; Li, Y.; Xiao, M. Ultrafast Hole Transfer Mediated by Polaron Pairs in All-Polymer Photovoltaic Blends. *Nat. Commun.* **2019**, *10*, 398.

(25) Wang, R.; Zhang, C.; Li, Q.; Zhang, Z.; Wang, X.; Xiao, M. Charge Separation from an Intra-Moiety Intermediate State in the High-Performance Pm6:Y6 Organic Photovoltaic Blend. *J. Am. Chem. Soc.* **2020**, *142*, 12751.

(26) Meng, L.; Zhang, Y.; Wan, X.; Li, C.; Zhang, X.; Wang, Y.; Ke, X.; Xiao, Z.; Ding, L.; Xia, R.; et al. Organic and Solution-Processed Tandem Solar Cells with 17.3% Efficiency. *Science* **2018**, *361*, 1094.

(27) Yan, T.; Song, W.; Huang, J.; Peng, R.; Huang, L.; Ge, Z. 16.67% Rigid and 14.06% Flexible Organic Solar Cells Enabled by Ternary Heterojunction Strategy. *Adv. Mater.* **2019**, *31*, 1902210.

(28) Cui, Y.; Yao, H. F.; Zhang, J. Q.; Xian, K. H.; Zhang, T.; Hong, L.; Wang, Y. M.; Xu, Y.; Ma, K. Q.; An, C. B.; He, C.; Wei, Z. X.; Gao, F.; Hou, J. H. Single-Junction Organic Photovoltaic Cells with Approaching 18% Efficiency. *Adv. Mater.* **2020**, *32*, 1908205.

(29) Bin, H.; Yang, Y.; Zhang, Z.-G.; Ye, L.; Ghasemi, M.; Chen, S.; Zhang, Y.; Zhang, C.; Sun, C.; Xue, L.; Yang, C.; Ade, H.; Li, Y. 9.73% Efficiency Nonfullerene All Organic Small Molecule Solar Cells with Absorption-Complementary Donor and Acceptor. *J. Am. Chem. Soc.* **2017**, *139*, 5085.

(30) Bin, H.; Gao, L.; Zhang, Z.-G.; Yang, Y.; Zhang, Y.; Zhang, C.; Chen, S.; Xue, L.; Yang, C.; Xiao, M.; Li, Y. 11.4% Efficiency Non-Fullerene Polymer Solar Cells with Trialkylsilyl Substituted 2d-Conjugated Polymer as Donor. *Nat. Commun.* **2016**, *7* (13651), 13651.
(31) Cui, Y.; Yao, H.; Zhang, J.; Zhang, T.; Wang, Y.; Hong, L.; Xian, K.; Xu, B.; Zhang, S.; Peng, J.; Wei, Z.; Gao, F.; Hou, J. Over 16% Efficiency Organic Photovoltaic Cells Enabled by a Chlorinated Acceptor with Increased Open-Circuit Voltages. *Nat. Commun.* **2019**, *10*, 2515.
(32) Zhang, J.; Tan, H. S.; Guo, X.; Facchetti, A.; Yan, H. Material Insights and Challenges for Non-Fullerene Organic Solar Cells Based on Small Molecular Acceptors. *Nat. Energy* **2018**, *3*, 720.
(33) Sun, C.; Qin, S.; Wang, R.; Chen, S.; Pan, F.; Qiu, B.; Shang, Z.; Meng, L.; Zhang, C.; Xiao, M.; Yang, C.; Li, Y. High Efficiency Polymer Solar Cells with Efficient Hole Transfer at Zero Highest Occupied Molecular Orbital Offset between Methylated Polymer Donor and Brominated Acceptor. *J. Am. Chem. Soc.* **2020**, *142*, 1465.
(34) Wang, R.; Yuan, J.; Han, G.; Huang, T.; Huang, W.; Xue, J.; Wang, H.-C.; Zhang, C.; Zhu, C.; Cheng, P.; Meng, D.; Yi, Y.; Wei, K.-H.; Zou, Y.; Yang, Y. Rational Tuning of Molecular Interaction and Energy Level Alignment Enables High-Performance Organic Photovoltaics. *Adv. Mater.* **2019**, *31*, 1904215.
(35) Best Research-Cell Efficiency Chart. https://www.nrel.gov/pv/cell-efficiency.html.
(36) Xu, T.; Yu, L. How to Design Low Bandgap Polymers for Highly Efficient Organic Solar Cells. *Mater. Today* **2014**, *17*, 11.
(37) Fan, Q.; Su, W.; Wang, Y.; Guo, B.; Jiang, Y.; Guo, X.; Liu, F.; Russell, T. P.; Zhang, M.; Li, Y. Synergistic Effect of Fluorination on Both Donor and Acceptor Materials for High Performance Non-Fullerene Polymer Solar Cells with 13.5% Efficiency, *Sci. Sci. China: Chem.* **2018**, *61*, 531.
(38) Lin, Y.; Adilbekova, B.; Firdaus, Y.; Yengel, E.; Faber, H.; Sajjad, M.; Zheng, X.; Yarali, E.; Seitkhan, A.; Bakr, O. M.; El-Labban, A.; Schwingenschlogl, U.; Tung, V.; McCulloch, I.; Laquai, F.; Anthopoulos, T. D. 17% Efficient Organic Solar Cells Based on Liquid Exfoliated Ws_2 as a Replacement for Pedot:Pss. *Adv. Mater.* **2019**, *31*, 1902965.
(39) Yu, R.; Yao, H.; Cui, Y.; Hong, L.; He, C.; Hou, J. Improved Charge Transport and Reduced Nonradiative Energy Loss Enable over 16% Efficiency in Ternary Polymer Solar Cells. *Adv. Mater.* **2019**, *31*, No. 1902302.
(40) Yuan, J.; Zhang, Y.; Zhou, L.; Zhang, G.; Yip, H.-L.; Lau, T.-K.; Lu, X.; Zhu, C.; Peng, H.; Johnson, P. A.; Leclerc, M.; Cao, Y.; Ulanski, J.; Li, Y.; Zou, Y. Single-Junction Organic Solar Cell with over 15% Efficiency Using Fused-Ring Acceptor with Electron-Deficient Core. *Joule* **2019**, *3*, 1140.
(41) Liu, Q.; Jiang, Y.; Jin, K.; Qin, J.; Xu, J.; Li, W.; Xiong, J.; Liu, J.; Xiao, Z.; Sun, K.; Yang, S.; Zhang, X.; Ding, L. 18% Efficiency Organic Solar Cells. *Sci. Bull.* **2020**, *65*, 272.
(42) Liu, X.; Zhang, C.; Duan, C.; Li, M.; Hu, Z.; Wang, J.; Liu, F.; Li, N.; Brabec, C. J.; Janssen, R. A. J.; Bazan, G. C.; Huang, F.; Cao, Y. Morphology Optimization Via Side Chain Engineering Enables All-Polymer Solar Cells with Excellent Fill Factor and Stability. *J. Am. Chem. Soc.* **2018**, *140*, 8934.
(43) Li, X.; Pan, F.; Sun, C.; Zhang, M.; Wang, Z.; Du, J.; Wang, J.; Xiao, M.; Xue, L.; Zhang, Z. G.; Zhang, C.; Liu, F.; Li, Y. Simplified Synthetic Routes for Low Cost and High Photovoltaic Performance N-Type Organic Semiconductor Acceptors. *Nat. Commun.* **2019**, *10*, 519.
(44) Sun, C.; Pan, F.; Bin, H.; Zhang, J.; Xue, L.; Qiu, B.; Wei, Z.; Zhang, Z.-G.; Li, Y. A Low Cost and High Performance Polymer Donor Material for Polymer Solar Cells. *Nat. Commun.* **2018**, *9*, 743.
(45) Gelinas, S.; Rao, A.; Kumar, A.; Smith, S. L.; Chin, A. W.; Clark, J.; van der Poll, T. S.; Bazan, G. C.; Friend, R. H. Ultrafast Long-Range Charge Separation in Organic Semiconductor Photovoltaic Diodes. *Science* **2014**, *343*, 512.
(46) Baran, D.; Gasparini, N.; Wadsworth, A.; Tan, C. H.; Wehbe, N.; Song, X.; Hamid, Z.; Zhang, W.; Neophytou, M.; Kirchartz, T.; Brabec, C. J.; Durrant, J. R.; McCulloch, I. Robust Nonfullerene Solar Cells Approaching Unity External Quantum Efficiency Enabled by Suppression of Geminate Recombination. *Nat. Commun.* **2018**, *9*, 2059.
(47) Lee, C.-L.; Hwang, I.-W.; Byeon, C. C.; Kim, B. H.; Greenham, N. C. Triplet Exciton and Polaron Dynamics in Phosphorescent Dye Blended Polymer Photovoltaic Devices. *Adv. Funct. Mater.* **2010**, *20*, 2945.
(48) Ginger, D. S.; Greenham, N. C. Photoinduced Electron Transfer from Conjugated Polymers to Cdse Nanocrystals. *Phys. Rev. B: Condens. Matter Mater. Phys.* **1999**, *59*, 10622.
(49) Yao, J.; Qiu, B.; Zhang, Z.-G.; Xue, L.; Wang, R.; Zhang, C.; Chen, S.; Zhou, Q.; Sun, C.; Yang, C.; Xiao, M.; Meng, L.; Li, Y. Cathode Engineering with Perylene-Diimide Interlayer Enabling over 17% Efficiency Single-Junction Organic Solar Cells. *Nat. Commun.* **2020**, *11*, 2726.
(50) Guo, J.; Ohkita, H.; Benten, H.; Ito, S. Charge Generation and Recombination Dynamics in Poly(3-Hexylthiophene)/Fullerene Blend Films with Different Regioregularities and Morphologies. *J. Am. Chem. Soc.* **2010**, *132*, 6154.
(51) Dutta, G. K.; Kim, T.; Choi, H.; Lee, J.; Kim, D. S.; Kim, J. Y.; Yang, C. Synthesis of Fluorinated Analogues of a Practical Polymer Tq for Improved Open-Circuit Voltages in Polymer Solar Cells. *Polym. Chem.* **2014**, *5*, 2540.
(52) Köhler, A.; Bässler, H. What Controls Triplet Exciton Transfer in Organic Semiconductors? *J. Mater. Chem.* **2011**, *21*, 4003.
(53) Han, G.; Hu, T.; Yi, Y. Reducing the Singlet-Triplet Energy Gap by End-Group Pi-Pi Stacking toward High-Efficiency Organic Photovoltaics. *Adv. Mater.* **2020**, *32*, 2000975.
(54) Burke, T. M.; Sweetnam, S.; Vandewal, K.; McGehee, M. D. Beyond Langevin Recombination: How Equilibrium between Free Carriers and Charge Transfer States Determines the Open-Circuit Voltage of Organic Solar Cells. *Adv. Energy Mater.* **2015**, *5*, 1500123.

https://dx.doi.org/10.1021/jacs.0c13352
J. Am. Chem. Soc. 2021, 143, 4359−4366